Tellus (1993), 45A, 193–200
Printed in Belgium – all rights reserved

TELLUS
ISSN 0280–6495

A numerical solution of the linear Rayleigh-Bénard convection equations with the *B*- and *C*-grid formulations

By WEIMIN XU and CHARLES A. LIN*, *Department of Atmospheric and Oceanic Sciences, and Center for Climate and Global Change Studies, McGill University, 805 Sherbrooke Street West, Montreal, Quebec, Canada H3A 2K6*

(Manuscript received 18 September 1992; in final form 5 January 1993)

ABSTRACT

The numerical solutions of the linear Rayleigh-Bénard convection equations using the Arakawa *B*- and *C*-grid formulations are compared with the analytic solution. The results show that the *C*-grid simulates better the growth rates of unstable modes. A convective parameterization is required when the horizontal grid size is larger than the horizontal scale of the most unstable mode, the latter being of the same order as the depth scale of the unstable stratification. Non-hydrostatic effects become important when the horizontal grid size is smaller than the scale of the unstable stratification.

1. Introduction

Convective instability can occur in both the atmosphere and ocean. In coarse resolution hydrostatic numerical models, the convective modes are not resolved, and their mixing effects are usually parameterized using convective adjustment. The convective scales can be explicitly resolved in high-resolution non-hydrostatic models. For the ocean, such models are usually formulated using the Arakawa (1972) *B*- and *C*-grids. In this note, we examine the effect of the 2 horizontal grid formulations and horizontal grid sizes on the simulation of Rayleigh-Bénard instability, by comparing their results to those obtained using analytic means. The importance of non-hydrostatic versus hydrostatic effects as a function of the horizontal resolution is also investigated. Martin and Pielke (1983) showed that the hydrostatic approximation remains valid in their study of sea-breeze modeling even when the aspect ratio is of order unity. A similar conclusion is found in the recent review of atmospheric convection by Molinari and Dudek (1992). It is thus of great interest to examine the role of non-hydrostatic effects in an oceanic context as well.

Arakawa and Lamb (1977), and Batteen and Han (1981) examined the effects of the 2 grids on the dispersive properties of inertial-gravity waves, which are essential for geostrophic adjustment. Their results show that for coarse grid (>100 km) ocean models, the *B*-grid performs better than the *C*-grid, while the opposite obtains at high resolution (<50 km). The critical parameter is the ratio of the Rossby radius of deformation to the grid size. Convective modes are buoyantly unstable modes; it is thus of interest to determine the performance of the 2 grids for the case of unstable stratification.

Davey and Whitehead (1981) investigated analytically convective instability in a 2-layer rotating fluid, and applied the results to sinking events in the ocean. They suggested that the horizontal scale of the fastest growing mode, found to be of the order of 500 m, may determine the scale of deep convection due to surface cooling. The effect of the earth's rotation is not important, except at small growth rates.

In this study, we use a numerical model to examine the effect of the *B*- and *C*-grid formulations on the convective instability of the linear

* Corresponding author.

Rayleigh-Bénard problem. The model formulation is presented in Section 2, the results in Section 3, and the conclusion in Section 4.

2. Model formulation

The linearized equations for the Rayleigh-Bénard problem are as follows:

$$u_t = -p_x/\rho_0 + fv + \nu \nabla^2 u, \tag{1}$$

$$v_t = -p_y/\rho_0 - fu + \nu \nabla^2 v, \tag{2}$$

$$\varepsilon w_t = -p_z/\rho_0 - g\rho'/\rho_0 + \varepsilon\nu \nabla^2 w, \tag{3}$$

$$T_t = (\Delta T/H)w + \kappa \nabla^2 T, \tag{4}$$

$$u_x + v_y + w_z = 0, \tag{5}$$

$$\rho' = -\alpha\rho_0 T. \tag{6}$$

The notation is standard: u, v, w are the velocity components in the east-west (x), north-south (y) and vertical (z) directions, respectively; t, p, ρ_0, ρ', f, g, ν, κ, α, ∇^2 denote time, pressure, reference density, perturbation density, constant Coriolis parameter, gravitational acceleration, viscosity, thermal diffusivity, thermal expansion coefficient, and the 3-dimensional Laplacian operator, respectively. The basic-state temperature has a linear distribution with a range of ΔT over the depth (H) of the channel. Stress-free boundary conditions ($u_z = v_z = 0$), together with vanishing normal velocity ($w = 0$) and temperature perturbation ($T = 0$), are used at the top and bottom boundaries ($z = 0,\ H$). The basic state is at rest with no horizontal variation of pressure and density. The multiplier ε takes on the value of either 0 or 1, corresponding to the hydrostatic and non-hydrostatic cases, respectively.

We may assume solutions to (1)–(6) of the following form:

$$[u, v, p] = [U, V, P]\cos(\pi mz/H)e^{i(kx+ly)+\lambda t}, \tag{7}$$

$$[w, T, \rho'] = [W, T^*, \rho^*]\sin(\pi mz/H)e^{i(kx+ly)+\lambda t}, \tag{8}$$

where k, l, m are wavenumbers in the x, y, and z directions; U, V, W, P and T^*, ρ^* are perturbation amplitudes. For unstable modes, $\lambda > 0$ is the growth rate. Substitution of eqs. (7), (8) in eqs. (1)–(6) together with the use of the boundary conditions yields an eigenvalue problem for the growth rate λ. The solution may be obtained analytically, as well as using B- and C-grid formulations. The arrangement for both grids is shown in Fig. 1. The horizontal velocities are carried at the same point for the B-grid, while this is not the case for the C-grid. The numerical solutions depend on the grid resolution δx, δy, δz; further details are presented in the Appendix. The nature of the solution depends on 3 physical dimensionless parameters:

$$\mathrm{Ra} = g\alpha\,\Delta T H^3/\nu\kappa,$$

$$\mathrm{Pr} = \nu/\kappa,$$

$$\mathrm{Ta} = f^2 H^4/\nu^2.$$

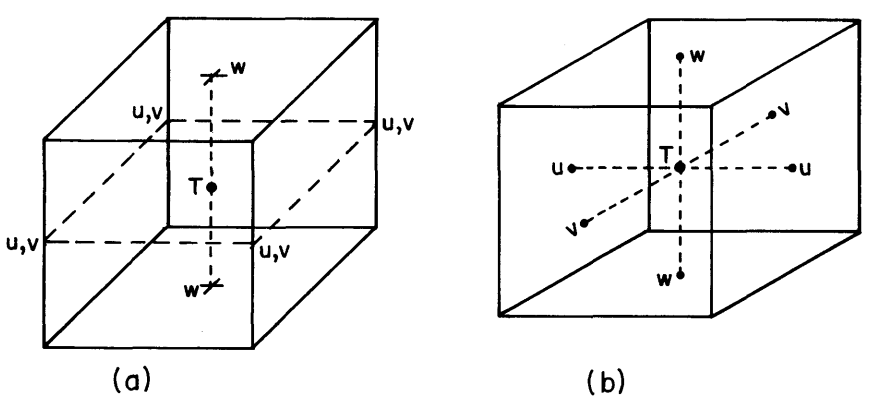

Fig. 1. The arrangement of velocity (u, v, w) and temperature (T) points in a grid box for the (a) B-grid, and (b) C-grid formulation.

The Rayleigh number (Ra) is a measure of the destabilizing temperature stratification ΔT relative to viscous and diffusive effects. The Prandtl number (Pr) is the ratio of the latter coefficients, while the Taylor number (Ta) is a measure of the rotation rate.

3. Results

The classic analytic solution (Chandrasekhar, 1961) of the Rayleigh-Bénard problem shows that unstable modes occur when the Rayleigh number is sufficiently large ($\mathrm{Ra} > 27\pi^4/4$), and that the vertical scale of the most unstable mode is that of the gravest mode ($m = 1$), with a horizontal scale of the same order.

We define the dimensionless wavenumbers k_0, l_0, m_0 as

$$k_0 = k\,\delta x/\pi, \qquad l_0 = l\,\delta y/\pi, \qquad m_0 = m\,\delta z/\pi.$$

A numerical model with a grid spacing of δx can only resolve a minimum wavelength of $2\delta x$. This, together with the absence of horizontal boundaries, means that the dimensionless horizontal wavenumbers k_0 and l_0 are constrained to have values between zero and unity. For simplicity, we take the 2 wavenumbers to be identical, $k_0 = l_0$, i.e., symmetry in the zonal and meridional directions is assumed. A limit on the smallest resolved scale is of course not present in the analytic model. In the vertical, the presence of boundaries at $z = 0$ and $z = H$ determines the vertical scale of the gravest mode as $m = \pi/H$. This means that the dimensionless wavenumber $m_0 > \delta z/H$, for both the analytic and numerical models.

In order to compare more readily the wavenumbers of the analytic and numerical models, we define the rescaled wavenumbers as

$$k_{00} = k_0(H/\delta x), \qquad l_{00} = l_0(H/\delta y),$$
$$m_{00} = m_0(H/\delta z).$$

Note that $H/\delta x$, $H/\delta y$ and $H/\delta z$ are measures of the horizontal and vertical resolutions of the numerical model. As k_0, l_0 have values less than unity, this means that k_{00} and l_{00} are smaller than $H/\delta x$ and $H/\delta y$, respectively. For basin scale ocean circulation models used for climate studies, δz is of the same order as $H/10$. We will compare the results for the *B*- and *C*-grid formulations ranging from low ($\delta x = 10H$) to high ($\delta x = H/10$) horizontal resolution. For subsequent results, we take $\mathrm{Ra} = 10^7$, $\mathrm{Pr} = 1$ and $\mathrm{Ta} = 10^2$, and identical grid spacings in the zonal and meridional directions ($\delta x = \delta y$), and $\delta z = H/10$.

Fig. 2 shows the growth rate of the unstable modes of the 3-dimensional non-hydrostatic ($\varepsilon = 1$) analytic model, as a function of the horizontal and vertical wavenumbers; its derivation is given in the Appendix. As noted earlier, the most unstable mode is the gravest mode in the vertical ($m_{00} = 1$) with its horizontal scale of the same order as the vertical scale. The horizontal scales which are actually resolved by the horizontal grid spacings of $\delta x = 10H$, H and $H/10$, are also indicated in Fig. 2. We see that the former 2 grid spacings do not resolve the most unstable mode. However, even for these cases, it is of interest to compare the performance of the 2 grid formulations in simulating the growth rates of the unstable modes.

Fig. 3 shows the growth rates at high horizontal resolution ($\delta x = H/10$) for the non-hydrostatic

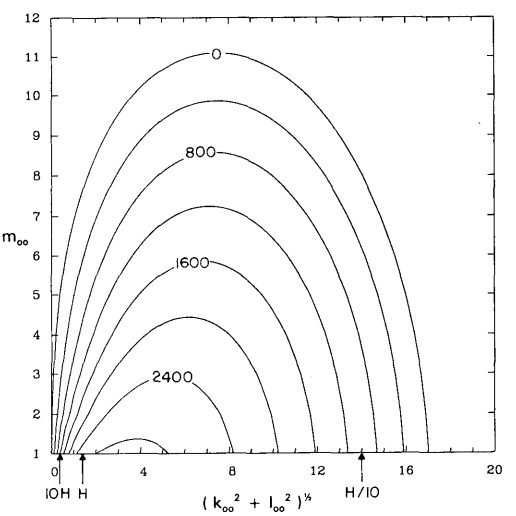

Fig. 2. The dimensionless growth rate ($\lambda H^2/\kappa$) of the unstable mode as a function of the dimensionless horizontal $[(k_{00}^2 + l_{00}^2)^{1/2}]$ and vertical (m_{00}) wavenumbers, from the analytic model. The resolution corresponding to the grid sizes of $\delta x = \delta y = 10H$, H and $H/10$ is shown by the arrow on the abcissa; only modes to the left of the arrow are resolved by the respective numerical model in these cases.

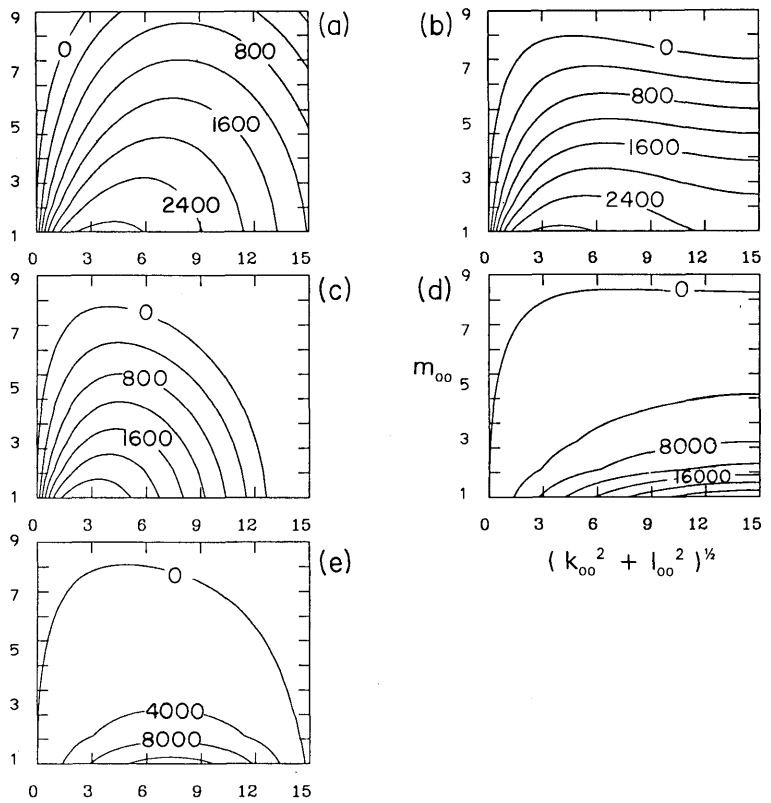

Fig. 3. The growth rate ($\lambda H^2/\kappa$) as a function of the horizontal $[(k_{00}^2 + l_{00}^2)^{1/2}]$ and vertical (m_{00}) wavenumbers, for the analytic and numerical models, with $\delta x = \delta y = H/10$ and $\delta z = H/10$: (a) analytic; (b) non-hydrostatic *C*-grid; (c) non-hydrostatic *B*-grid; (d) hydrostatic *C*-grid; (e) hydrostatic *B*-grid.

analytic model, and the hydrostatic and non-hydrostatic numerical models. We first note that in the limit of infinitely high resolution, the results of the *B*- and *C*-grids both converge to the non-hydrostatic analytic case; this has been verified by increasing the horizontal resolution beyond $\delta x = H/10$ (figures not shown). The most unstable mode is resolved at the latter resolution (Fig. 2), but the behaviour of the two grid formulations differ. For the non-hydrostatic case, the *C*-grid (Fig. 3b) simulates a larger range of unstable horizontal scales compared to the *B*-grid (Fig. 3c), and this is in better agreement with the analytic results (Fig. 3a). Indeed, the *B*-grid yields a high wavenumber cutoff which is not present in the analytic results at these wavelengths. In addition, the growth rate of the most unstable mode is underestimated more by the *B*-grid. This is probably due to the dissipative nature of the grid-point averaging needed to calculate the horizontal pressure gradient in the *B*-grid formulation. The hydrostatic numerical results (Figs. 3d, e) for both grids give completely incorrect growth rates; this is expected for high horizontal resolution, where non-hydrostatic effects become important.

The results for coarser horizontal resolution are shown in Fig. 4 ($\delta x = H$) and Fig. 5 ($\delta x = 10H$). Note that the most unstable mode is no longer resolved at these resolutions (Fig. 2). However, the *B*-grid simulations show a most unstable mode (Figs. 4c and 5c), with a growth rate which is much smaller than the analytic results (Figs. 4a and 5a). In contrast, the *C*-grid performs much better: the growth rate distribution and its magnitude (Figs. 4b, 5b) are both simulated well. We also note that the non-hydrostatic and hydrostatic results for the

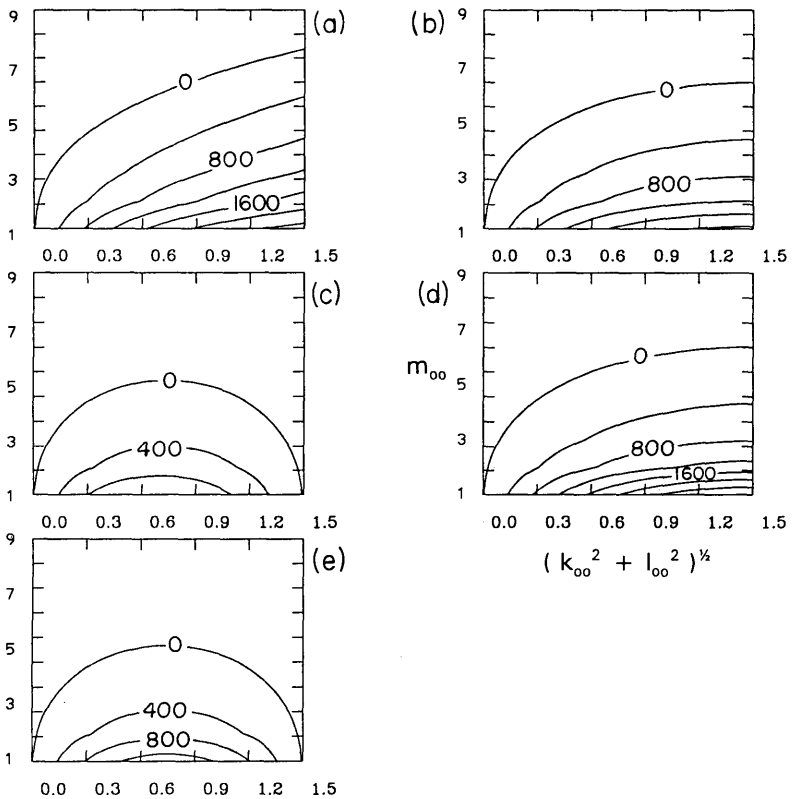

Fig. 4. As Fig. 3, but for $\delta x = \delta y = H$.

2 respective grids are now similar, due to the coarse horizontal resolution used in these cases.

Davey and Whitehead (1981, hereafter referred to as DW), performed an analytic linear stability analysis using a statically unstable two-layer fluid system. Their results suggest a preferred horizontal scale of about 500 m for deep convection events due to surface cooling in the ocean. To simplify the analysis, they did not consider the effects of vertical viscosity. We now estimate the value of the Rayleigh number implied by the choice of the degree of static instability in their model. The latter is measured by the reduced gravity parameters $g' = (\delta\rho/\rho_0)\, g$, where $\delta\rho = \rho_2 - \rho_1$ is the density difference between the 2 layers, and ρ_0 is a reference density value. The magnitude of $\delta\rho$ is small compared to ρ_0, and $\delta\rho < 0$ for static instability. The depths of the two layers are H_1 and H_2. DW estimated a representative value of $g' = -10^{-5}\,\mathrm{m\,s^{-2}}$, corresponding to typical cooling events in the upper ocean, with depths $H_1 = 100$ m and $H_2 = 1000$ m, respectively. To determine an equivalent Rayleigh number, we note that the corresponding temperature stratification is $\delta T = -(g'/g)T_0$, for some reference temperature T_0. This temperature difference occurs over the depth H, which is taken to be the geometric mean of H_1 and H_2; this is of course a crude assumption, as it is not strictly possible to approximate a 2-layer system with a linear profile. This then leads to a value $\mathrm{Ra} = 6 \times 10^7$, with $\alpha = 2.5 \times 10^{-4}\,{}^{0}\mathrm{C}^{-1}$, $\nu = \kappa = 10^{-4}\,\mathrm{m^2\,s^{-1}}$. This is comparable to the value of $\mathrm{Ra} = 10^7$ that we used in the analysis of the performance of the *B*- and *C*-grids. Our results do not change substantially for $\mathrm{Ra} = 10^6$ or 10^8, although the growth rates do increase with the Rayleigh number. We have used identical values of the horizontal and vertical eddy viscosities, which is typical of the vertical viscosity in numerical ocean models. In the latter, the

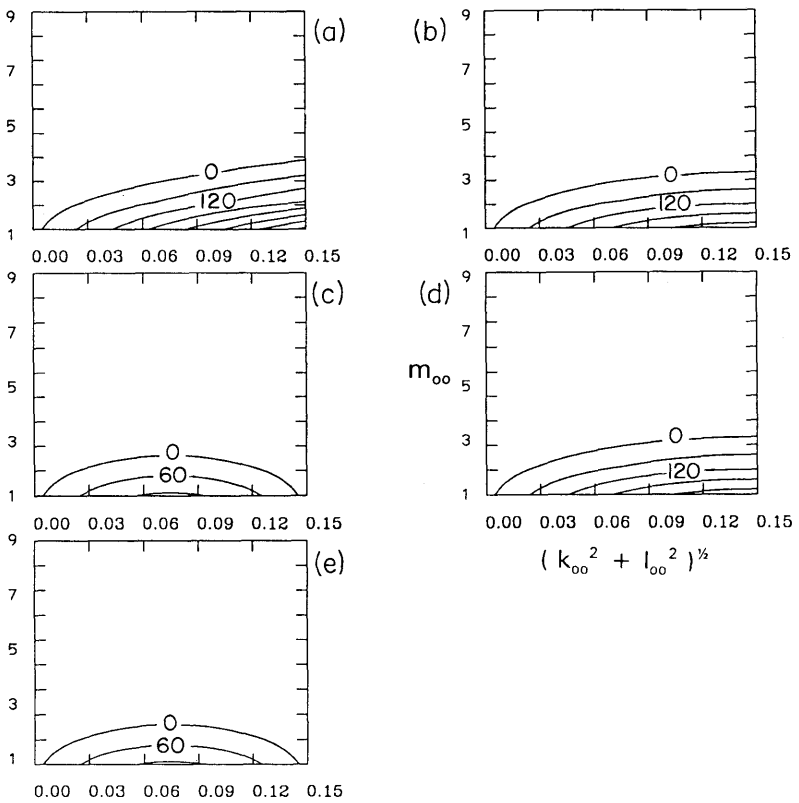

Fig. 5. As Fig. 3, but for $\delta x = \delta y = 10H$.

horizontal viscosity is many orders larger than the vertical value, due to the use of a coarser horizontal resolution compared to the vertical resolution. However, the horizontal contribution to the Laplacian term, which consists of the product of the horizontal viscosity and the horizontal gradient of the velocity shear, remains comparable to the vertical contribution, due to the coarse horizontal resolution ($\Delta x \gg \Delta z$) in such models. This means that the Laplacian diffusion is almost isotropic. In our high horizontal resolution case ($\Delta x = H/10 = \Delta z$), the horizontal and vertical resolutions are equal; there is thus no reason to use a much larger horizontal viscosity. For the intermediate and low horizontal resolution cases ($\Delta x = H$, $10H$; $\Delta z = H/10$), the use of equal horizontal and vertical viscosities means that the former is underestimated compared to that found in numerical models. The use of a larger horizontal viscosity in these cases would severely damp the convective modes, with the *C*-grid still performing better than the *B*-grid. We have thus chosen to use identical values of the horizontal and vertical viscosities.

DW also showed that except for small growth rates found near marginal instability, the effects of the earth's rotation are not important. Thus, the choice of the Taylor number Ta is not crucial; this has been verified in our analysis. We have used a value of $\mathrm{Ta} = 10^2$ throughout this study, which corresponds to weak rotation compared to the earth's rotation. Increasing Ta would increase the critical value of the Rayleigh number for the onset of instability, and the result that the *C*-grid performs better than the *B*-grid still remains valid. Increasing the Prandtl number would increase the growth rate; the *C*-grid performs better than the *B*-grid in these cases as well (figures not shown).

4. Conclusions

We have examined the numerical solutions to the classic Rayleigh-Bénard problem in the hydrostatic and non-hydrostatic limits, using both the Arakawa *B*- and *C*-grid formulations. The results have been compared with the analytic solution. The relevant dimensionless parameters are the Rayleigh (Ra), Prandtl (Pr) and Taylor (Ta) numbers, as well as the grid resolution relative to the depth of the fluid ($\delta x/H$, $\delta y/H$, $\delta z/H$).

The most unstable mode is resolved in the non-hydrostatic case when sufficiently high horizontal resolution is used ($\delta x < H$). Conversely, at coarse horizontal resolution ($\delta x > H$), the hydrostatic and non-hydrostatic results become closer. The most unstable mode has horizontal and vertical scales of the same order, is thus not resolved in both cases. This in turn means that a convective adjustment parameterization is required in coarse horizontal resolution models, in both the hydrostatic and non-hydrostatic cases.

In general, the *C*-grid performs better than the *B*-grid in simulating the growth rate of convectively unstable modes. Note that in the Batteen and Han (1981) study of geostrophic adjustment, the *C*-grid also worked better for the frequency of inertial-gravity waves, when the horizontal resolution is smaller than the first modal Rossby radius of deformation.

A difficulty with the simulation of convectively unstable modes in a numerical model is that such instability can occur at any scale, down to that of the grid resolution. We have circumvented this in our study by taking the grid resolution to be less than the scale of the instability ($\delta z < H$), thus allowing the resolution of unstable modes at sufficiently high horizontal resolution. In such cases, the *C*-grid performs better than the *B*-grid. This conclusion is of interest as progressively higher horizontal resolution is used in eddy-resolving ocean circulation models (Holland, 1989).

5. Appendix

Substituting the wave-form solutions given in eqs. (7)–(8) in the linearized eqs. (1)–(6), we obtain the following set of eigenvalue equations for the growth rate λ:

$$[a_{11}-\lambda]U + a_{12}V + a_{13}T^* = 0,$$

$$a_{21}U + [a_{22}-\lambda]V + a_{23}T^* = 0,$$

$$a_{31}U + a_{32}V + [a_{33}-\lambda]T^* = 0.$$

The coefficients $\{a_{ij}\}$ assume different values for the analytic and numerical models. For the analytic model, we have

$$a_{11} = -n^2\nu, \qquad a_{23} = 0,$$

$$a_{12} = -(m/n^2)f, \qquad a_{31} = \Delta T/H,$$

$$a_{13} = g\alpha(k^2+l^2)/n^2, \qquad a_{32} = 0,$$

$$a_{21} = mf, \qquad a_{33} = -n^2\kappa.$$

$$a_{22} = -n^2\nu,$$

In the above, $n^2 = k^2 + l^2 + m^2$ is the 3-dimensional wavenumber. The convective growth rate λ is then obtained as an eigenvalue.

For the numerical model, the coefficients $\{a_{ij}\}$ are given by the following relations.

$$a_{11} = \mathrm{Pr}H^2 d = a_{22},$$

$$a_{33} = H^2 d,$$

$$a_{12} * a_{21} = -b^2\mathrm{TaPr}^2,$$

$$a_{13} * a_{31} = (a_1^2 c^2/a_3^2)\mathrm{RaPr},$$

$$a_{23} * a_{32} = (a_2^2 c^2/a_3^2)\mathrm{RaPr},$$

$$a_{13} * a_{32} * a_{21} = -(a_1 a_2 c^2 b/a_3^2)\mathrm{RaPr}^2\mathrm{Ta}^{1/2},$$

$$a_{31} * a_{12} * a_{23} = (a_1 a_2 c^2 b/a_3^2)\mathrm{RaPr}^2\mathrm{Ta}^{1/2}.$$

The above equations relate the coefficients to the dimensionless numbers Ra, Pr, Ta, the depth of the fluid H, and the parameters a_1, a_2, a_3, b, c, d. The values of the latter 6 parameters depend on whether the hydrostatic approximation is made, and the grid scheme used; they are shown below.

(1) Hydrostatic *C*-grid model:

$$a_1 = \sin(k\,\delta x/2)/\delta x,$$

$$a_2 = \sin(l\,\delta y/2)/\delta y,$$

$$a_3 = \sin(m\,\delta z/2)/\delta z,$$

$$b = \cos(k\,\delta x/2)\cos(l\,\delta y/2),$$

$$c = \cos(m\,\delta z/2),$$

$$d = -(a_1^2 + a_2^2 + a_3^2).$$

(2) Hydrostatic B-grid model:

$a_1 = 2\sin(k\,\delta x/2)\cos(l\,\delta y/2)/\delta x,$

$a_2 = 2\cos(k\,\delta x/2)\sin(l\,\delta y/2)/\delta y,$

$a_3 = 2\sin(m\,\delta z/2)/\delta z,$

$b = 1,$

$c = \cos(m\,\delta z/2),$

$d = -(a_1^2 + a_2^2 + a_3^2).$

(3) Non-hydrostatic B- and C-grid models:

The non-hydrostatic solutions of B- and C-grid models are the same as the corresponding hydrostatic counterparts except

$a_{11} = \mathrm{Pr}H^2 d + h_1,$

$a_{22} = \mathrm{Pr}H^2 d - h_1,$

$a_{33} = H^2 d,$

$a_{12} * a_{21} = -h_2 h_3 b^2 \mathrm{TaPr}^2,$

$a_{13} * a_{31} = (a_1^2 c^2/d)\mathrm{RaPr},$

$a_{23} * a_{32} = (a_2^2 c^2/d)\mathrm{RaPr},$

$a_{13} * a_{32} * a_{21} = -(a_1 a_2 c^2 b/d)h_1 \mathrm{RaPr}^2\mathrm{Ta}^{1/2},$

$a_{31} * a_{12} * a_{23} = (a_1 a_2 c^2 b/d)h_2 \mathrm{RaPr}^2\mathrm{Ta}^{1/2},$

and where

$h_1 = -a_1 a_2 b/d,$

$h_2 = 1 - a_2^2/d,$

$h_3 = 1 - a_2^2/d.$

Acknowledgments

Helpful discussion with Dr. D. L. Zhang during the course of this work is gratefully acknowledged. Ms. U. Seidenfuss helped in the preparation of the figures. Financial support is provided by the Natural Sciences and Engineering Research Council (NSERC), and the Atmospheric Environment Service (AES) of Canada. The preparation of this work was aided by the computational facilities of CERCA (Centre de Recherche en Calcul Appliqué). Helpful comments from 2 anonymous referees, which improved the manuscript, are gratefully acknowledged.

REFERENCES

Arakawa, A. 1972. *Numerical simulation of weather and climate*, Technical Report no. 7. Department of Meteorology, University of California, Los Angeles, USA.

Arakawa, A. and Lamb, V. R. 1977. Computational design of the basic dynamical processes of the UCLA general circulation model. In: *Methods of computational physics*, vol. 17. Academic Press, New York, 173–265.

Batteen, M. L. and Han, Y.-J. 1981. On the computational noise of finite difference schemes used in ocean models. *Tellus 33*, 387–396.

Chandrasekhar, S. 1961. *Hydrodynamic and hydromagnetic stability*. Dover Press, New York, USA, 645 pp.

Davey, M. K. and Whitehead, J. A., Jr. 1981. Rotating Rayleigh-Taylor instability as a model of sinking events in the ocean. *Geophys. Astrophys. Fluid Dynamics 17*, 237–253.

Holland, W. R. 1989. Experiences with various parameterizations of subgrid scale dissipation and diffusion in numerical models of ocean circulation. In: *Parameterization of small-scale processes*, Proceedings of Aha Huliko'a Winter Workshop, 1989, P. Muller and D. Henderson (eds.). Hawaii Institute of Geophysics, Hawaii, USA, pp. 99–116.

Martin, C. L. and Pielke, R. 1983. The adequacy of the hydrostatic assumption in sea breeze modeling over flat terrain. *J. Atmos. Sci. 40*, 1472–1481.

Molinari, J. and Dudek, M. 1992. Parameterization of convective precipitation in mesoscale numerical models: a critical review. *Mon. Wea. Rev. 120*, 326–344.